Embryo fossilization is a biological process mediated by microbial biofilms

Elizabeth C. Raff[a,b,1], Kaila L. Schollaert[a], David E. Nelson[a], Philip C. J. Donoghue[c], Ceri-Wyn Thomas[c], F. Rudolf Turner[a], Barry D. Stein[a], Xiping Dong[d], Stefan Bengtson[e], Therese Huldtgren[e,f], Marco Stampanoni[g,h] Yin Chongyu[i], and Rudolf A. Raff[a,b,1]

[a]Department of Biology and Indiana Molecular Biology Institute, Indiana University, Bloomington, IN 47405; [b]School of Biological Sciences, University of Sydney, Sydney NSW 2006, Australia; [c]Department of Earth Sciences, University of Bristol, Bristol BS8 1RJ, United Kingdom; [d]Department of Earth and Space Sciences, Peking University, Beijing 100871, Peoples Republic of China; [e]Department of Palaeozoology, Swedish Museum of Natural History, SE-104 05 Stockholm, Sweden; [f]Department of Geology and Geochemistry, Stockholm University, SE-106 91 Stockholm, Sweden; [g]Swiss Light Source, Paul Scherrer Institut, 5232 Villigen, Switzerland; [h]Institute for Biomedical Engineering, University and ETH Zürich, Zürich, Switzerland; and [i]Institute of Geology, Chinese Academy of Geological Sciences, Beijing 100864, Peoples Republic of China

Communicated by James W. Valentine, University of California, Berkeley, CA, October 9, 2008 (received for review August 19, 2008)

Fossilized embryos with extraordinary cellular preservation appear in the Late Neoproterozoic and Cambrian, coincident with the appearance of animal body fossils. It has been hypothesized that microbial processes are responsible for preservation and mineralization of organic tissues. However, the actions of microbes in preservation of embryos have not been demonstrated experimentally. Here, we show that bacterial biofilms assemble rapidly in dead marine embryos and form remarkable pseudomorphs in which the bacterial biofilm replaces and exquisitely models details of cellular organization and structure. The experimental model was the decay of cleavage stage embryos similar in size and morphology to fossil embryos. The data show that embryo preservation takes place in 3 distinct steps: (*i*) blockage of autolysis by reducing or anaerobic conditions, (*ii*) rapid formation of microbial biofilms that consume the embryo but form a replica that retains cell organization and morphology, and (*iii*) bacterially catalyzed mineralization. Major bacterial taxa in embryo decay biofilms were identified by using 16S rDNA sequencing. Decay processes were similar in different taphonomic conditions, but the composition of bacterial populations depended on specific conditions. Experimental taphonomy generates preservation states similar to those in fossil embryos. The data show how fossilization of soft tissues in sediments can be mediated by bacterial replacement and mineralization, providing a foundation for experimentally creating biofilms from defined microbial species to model fossilization as a biological process.

bacterial | developmental evolution | metazoan origins | taphonomy | Cambrian

Fossilized embryos from the Late Proterozoic and Cambrian provide the only direct insight into embryology during the emergence of animal phyla (1–5). These fossils exhibit exceptional preservation of cell geometry and cytological structure. However, the mechanism of fossilization is not well understood. It has been hypothesized from fossil evidence that microbial processes are responsible for preservation and mineralization of organic tissues, and experimental studies have revealed insights into mineralization conditions (6–9). However, how bacteria and biofilms function in the preservation of embryo structure has not been observed and experimentally studied. We have carried out experimental taphonomy by using early stage embryos from the Australian sea urchin *Heliocidaris erythrogramma* (Fig. 1 *A* and *B*) that resemble Neoproterozoic and Cambrian fossil embryos in general features of cell morphology and size (10). Our results illuminate the processes of decay, preservation, and mineralization of animal embryos, as well as biases in preservation that may influence interpretations of developmental mode (10–12).

Here, we report experiments in which we examined decay under a variety of aerobic and anaerobic conditions to determine the conditions under which fossilization with the fine preservation of cellular morphology that is evident in some fossil embryos can occur. We show that embryo taphonomy is the product of 3 distinct processes. First, and most rapid, is autolysis, the self-destruction of cells within hours under aerobic conditions by their own lytic enzymes (11, 12). Thus, preservation sufficient for potential fossilization with preservation of tissue and cell structure requires that there were conditions in ancient marine environments that provided a rapid block to autolysis on death of the embryo. Second, during decay, bacteria invade and consume the embryo. We found that biofilms formed by invading bacterial communities maintain embryo form by pseudomorphing biological structures. Third, bacteria also produce changes in embryo chemistry that affect mineralization potential; thus, rapid formation of fine-grain mineralization may be catalyzed by biofilm bacteria (8). We identify major bacterial taxa involved with the 2 latter processes.

Results

Autolysis Versus Bacterial-Mediated Preservation. Cell boundaries and cellular structures are rapidly degraded after death if autolysis is not blocked (Fig. 1*C*). Thus, for fossilization of embryo structures to occur, the conditions for fossilization must block autolysis, which experimentally can be prevented by reducing conditions (produced by addition of 100 mmol of β-mercaptoethanol) (11, 12), or anaerobic conditions (see *Materials and Methods*). Evidence that compatible conditions obtained during the initial stages of metazoan fossilization is apparent in the sediments from which fossilized embryos have been recovered (13). Bacterial growth, but not autolysis, could be blocked by the broad-spectrum antibiotic rifampicin. When both autolysis and microbial activity were blocked, embryos did not undergo any perceivable structural degradation in either aerobic or anaerobic conditions. Bacterial action is therefore the primary mediator of all taphonomic processes except autolysis.

Bacterial Biofilms Preserve Details of Cellular Structure by Generating Pseudomorphs of Embryos. Biofilms are 3-dimensional aggregations of bacteria within a cohesive hydrated exopolysaccharide matrix (14). In our experiments, embryo structure provides the template on which bacterial biofilms form. The biofilm replaces, replicates, and stabilizes the complete morphology of the consumed embryo in fine detail. The effects of experimental

Author contributions: E.C.R., D.E.N., P.C.J.D., and R.A.R. designed research; E.C.R., K.L.S., P.C.J.D., C.-W.T., F.R.T., B.D.S., X.D., S.B., T.H., M.S., and R.A.R. performed research; P.C.J.D., X.D., S.B., M.S., and Y.C. contributed new reagents/analytic tools; E.C.R., K.L.S., D.E.N., P.C.J.D., C.-W.T., T.H., M.S., and R.A.R. analyzed data; and E.C.R., D.E.N., P.C.J.D., S.B., and R.A.R. wrote the paper.

The authors declare no conflict of interest.

[1]To whom correspondence may be addressed. E-mail: raff@indiana.edu or raffr@indiana.edu.

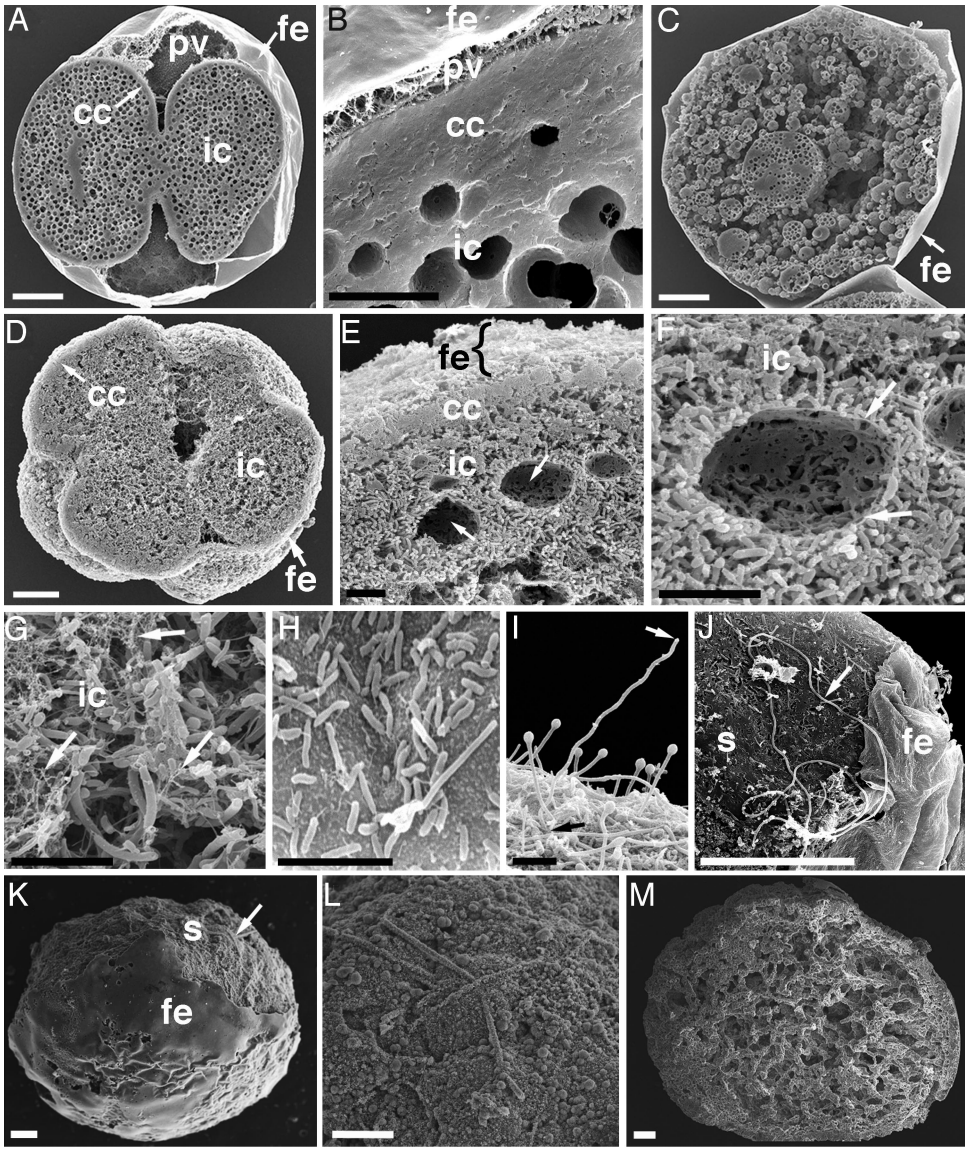

Fig. 1. Taphonomic patterns in embryos. Scanning electron micrographs. (*A–J*) Experimental taphonomy of *Heliocidaris erythrogramma* embryos. All embryos except C killed as in *A*. (*A–G*) Freeze-fractured. (*A*) Embryo killed during second cleavage with seawater containing 100 mmol of β-mercaptoethanol (BME); fixed at 18 h. Cell structure and organization are intact: fe, fertilization envelope; pv, perivitelline space; cc, dense cortical cytoplasm; ic, inner cytoplasm with numerous lipid vesicles (lipids extracted by sample preparation). (*B*) Cytoplasmic layers in similar control embryo. (*C*) Two-cell embryo killed by 10 min in seawater containing 1% NH_4 (11); fixed after 24 h in seawater containing rifampicin. Fertilization envelope is intact, but autolysis has destroyed internal structure. (*D*) Five days in standard aerobic decay conditions (*Materials and Methods*). Bacteria have consumed the embryo, but resulting biofilms preserve cell organization. Fertilization envelope is closely apposed to embryo surface. (*E*) Three days decay in seawater with no reducing agents; bacterially replicated cytoplasmic layers retain morphology and lipid vesicles (arrows). (*F*) Embryo E, internal cytoplasm with extracellular matrix of the bacterial biofilm visible at lipid vesicle surface (arrows). (*G*) Embryo D, internal cytoplasm showing extracellular matrix fibers of the bacterial biofilm (arrows). (*H*) Fertilization envelope after 5 days in standard anaerobic decay conditions (*Materials and Methods*); anaerobic biofilm forming. (*i*) Dense biofilm on embryo surface after 5 days anaerobic decay with anaerobic mud inoculum (*Materials and Methods*). Filamentous bacterium extends 35 μm (arrows). (*J*) Four days anaerobic decay with anaerobic mud inoculum. Fertilization envelope partly covers the embryo surface (s). Filamentous bacterium (arrow) exceeds 300 μm. (*K–M*) Lower Cambrian phosphorite-preserved fossil embryos from Kuanchuanpu, China. (*K*) Embryo partly covered by presumptive fertilization envelope; exposed surface has filamentous structures (arrow). (*L*) Embryo K surface: 100- to 200-μm filaments among mineral spheroids. (*M*) Fossil embryo showing interior microfabric. (Scale bar: *A*, *C*, *D*, *J–M*, white, 50 μm; *B*, *E–I*, black, 5 μm).

biofilms on embryos are shown in Fig. 1. A section of a freshly killed embryo shows a number of structural elements, including the fertilization envelope, the perivitellin space between embryo and fertilization envelope, the overall form of the embryonic cells, and the cytoplasmic structures of cell boundaries, inner and outer cytoplasms, and cytoplasmic inclusions, here, lipid vesicles (Fig. 1 *A* and *B*). When autolysis is blocked, killed embryos maintained in seawater are colonized by marine bacteria, which rapidly consume embryonic substance and replace it with a biofilm (Fig. 1*D*). The surprising observation is that such embryos constitute bacterial pseudomorphs that retain embryonic structure with fidelity (Fig. 1 *D–G*). Fertilization envelope and overall cell form are gross morphological features. However, smaller cytoplasmic structures such as lipid vesicles are also modeled by bacteria and biofilm extracellular material.

Patterns of bacterial growth depend on incubation conditions. Both aerobic and anaerobic conditions allow biofilm formation, but the bacterial constituents are different (Fig. 1 *H–J*). Under

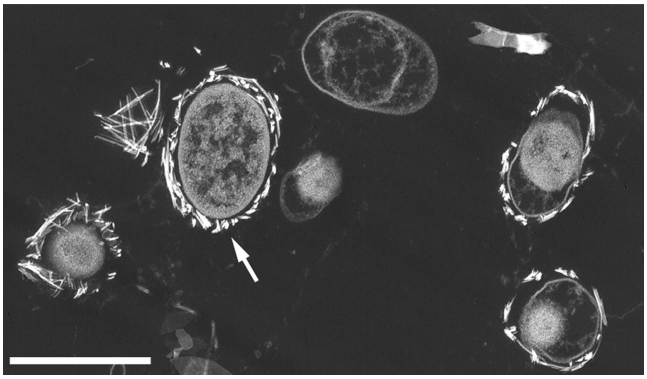

Fig. 2. Bacterial mineralization in experimental taphonomy of *H. tuberculata* embryos. Transmission electron micrograph of surface bacteria from an *H. tuberculata* embryo with autolysis blocked by 100 mmol of BME, then decayed for 6 days under standard aerobic conditions (*Materials and Methods*). Acicular crystals have formed around some of the bacteria in the surface biofilm (arrow). (Scale bar: 1 μm).

anaerobic conditions, long filamentous forms appear (Fig. 1 *I* and *J*). When autolysis was blocked and bacterial growth occurred, the progress of bacterial replacement followed the same pattern in all of the conditions we tested, with condition-dependent differences in timing and bacterial populations. Aerobic bacterial growth was faster than anaerobic growth, and faster in the absence of the reducing agent β-mercaptoethanol. Anaerobic bacterial growth was faster and more complex in the presence of an anerobic mud inoculum, which provided complex environmentally derived bacterial populations distinct from the bacteria associated with embryos or present in seawater. In all cases, patches of bacteria first appear on the surface of the fertilization envelope (Fig. 1*H*), eventually penetrating the embryo. The filamentous bacteria seen under anaerobic conditions resemble filamentous forms preserved in Cambrian fossil embryos (Fig. 1 *K–M*). The biofilm and its extracellular matrix then potentially provide the template for mineralization.

Bacterial Catalysis of Mineralization. In addition to *H. erythrogramma* embryos, we tested experimental taphonomic conditions on the smaller (90 μm) embryos of *H. tuberculata*. The mode of decay processes were the same in the smaller embryos, but proceeded faster. Acicular 15–400-nm crystals formed around bacteria on the surface of *H. tuberculata* embryos after 6 days aerobic decay (Fig. 2). Electron diffraction analyses indicate that the structure of the crystals is consistent with aragonite. Extracellular polymeric substances are known to induce diagenetic mineralization, possibly as the result of the liberation of adsorbed cations during degradation (15–17). Precipitation of calcium carbonate versus calcium phosphate is controlled by the local environment, governed by decay-induced pH. Higher pH favors calcium carbonate, with a fall in pH triggering a switch to calcium phosphate (18). Fossil embryos are preserved by calcium phosphate replacement. Thus, our experimental taphonomic conditions are compatible with initiation of mineralization by bacteria in the biofilms associated with decaying embryos, a necessary precondition for eventual fossilization.

Identification of Biofilm Bacteria in Embryo Decay Processes. The different bacterial forms in aerobic and anaerobic conditions indicate distinct bacterial floras and metabolic capabilities. We identified bacteria in the experimental embryo biofilms by cloning and sequencing bacterial 16S rRNA genes from total DNA prepared from embryos held under several taphonomic conditions (19). Table 1 shows the complete spectrum of bacteria identified in 1 aerobic and 2 different anaerobic taphonomic conditions. Fig. 3 summarizes the bacterial taxa represented in the different conditions. The analysis reveals that gamma proteobacteria, primarily *Pseudoalteromonas* and *Vibrio* species, make up the bulk of the biofilm under aerobic conditions.

Pseudoalteromonas is also prevalent in embryos incubated in anaerobic seawater (Fig. 1*H*), consistent with the reported capability of *Pseudoalteromonas* species for facultative anaerobic growth (20). Embryos held in anaerobic seawater with an inoculum of anaerobic mud contain primarily long filamentous bacteria, likely belonging to the Bacteriodetes phylum. *Pseudoalteromonas* is reported to be a primary marine biofilm colonizer, with additional species joining in after the initiation of a biofilm (21). Moreover, *Pseudoalteromonas* and related *Vibrio* are frequently associated with marine embryos (22). We therefore suggest that the course of biofilm development in all of our samples involves initial biofilm formation by *Pseudoalteromonas* carried by the embryos themselves. In anaerobic samples incubated with mud, the initial biofilm is overgrown by filamentous and other bacteria.

Discussion

Exquisitely preserved fossil microbial biofilms retaining bacterial forms are found in some soft animal tissue fossils of Mesozoic and Cenozoic ages (9, 23–25). The lower Cambrian embryo shown in Fig. 1 *K* and *L* has mineralized filamentous forms that resemble the filamentous anaerobic bacteria from taphonomic experiments (Fig. 1 *I* and *J*). Similar filaments have been observed in fossilized Neoproterozoic embryos from Doushantuo (2). Some fossil embryos show degraded interiors that resemble mineralized biofilm fabrics (Fig. 1*M*) (12), similar to the experimental taphonomic biofilm matrices (Fig. 1*F*). The majority of fossil embryos show no such interior fabric; however, internal bacteria might not be imaged even if preserved (4). The pattern of degradation of the embryos in our experiments matches the spectrum of preservation seen in fossil deposits such as Doushantuo (Fig. 4), ranging from specimens in which fine subcellular detail is preserved (Fig. 4 *B–D*), to forms in which cells may be distinguished on the outer surface, but there is little or no structure apparent in the inner mass of the embryo (Fig. 4*F*). The results of our experiments suggest that although fossils reflect their original embryological structure, they may in fact be fossilized bacterial pseudomorphs of that original structure. This preservational pathway likely limits the fidelity of structures that may be replicated by biofilms and, ultimately, by mineral.

Although microbial activity has always been implicated in decay and mineralization in fossil preservation of detailed cellular structure, previous studies have relied mainly on rare empirical evidence of fossilized bacteria. Our data provide direct evidence for microbial biofilms and identification of bacterial taxa involved in decay, pseudomorphing of cell structures, and potential for mineralization that can lead ultimately to exceptional fossilization. We recognize that even when microbes are present, mineralization of animal soft tissue may be produced abiogenically, for example, under conditions of high phosphate concentrations (26–28). The frequency of these mineralization modes remains to be determined for embryos. However, all fossil embryos show evidence of decay and, in the vast majority of cases, decay has been so considerable that only gross features such as the fertilization envelope or other outer coverings remain (12, 13, 29). Thus, embryo fossils are, to a greater or lesser degree, microbial pseudomorphs of the original cells and this fabric can be seen replicated in mineral. We suggest that bacterial biofilm formation within embryos is required in a substantial number of cases for both preservation of cell structure and subsequent bacteria-generated mineralization.

Experimental taphonomy has not yet addressed variations in microbial activity and composition, and metabolic capabilities.

Table 1. Identification of bacteria present during embryo decay.

Bacteria	Accession no.	Group	No. of Clones	% Identity
		Aerobic decay		
Pseudoalteromonas JL-96	AY745871.1	Gamma proteobacteria	14	95–99
Vibrio harveyi	CP000790.1	Gamma proteobacteria	2	98
Vibrio parahaemolyticus	BA000032.2	Gamma proteobacteria	1	99
Vibrio LAR2	DQ530291.1	Gamma proteobacteria	1	98
Vibrio S-11	DQ978992.1	Gamma proteobacteria	1	98
Vibrio V639	DQ146989.1	Gamma proteobacteria	1	99
Bacterium *K2–89o*	AY345481.1	Gamma proteobacteria	1	96
		Anaerobic decay		
Pseudoalteromonas JL-96	AY745871.1	Gamma proteobacteria	8	86–99
Vibrio parahaemolyticus	BA000032.2	Gamma proteobacteria	4	89–98
Vibrio harveyi	AY332404.1	Gamma proteobacteria	1	99
U. gamma proteobacterium (SC3–6)	DQ289936.1	Gamma proteobacteria	1	94
U. gamma proteobacterium (SIMO-4138)	DQ421503.1	Gamma proteobacteria	1	88
Marinomonas blandensis	DQ403809.1	Gamma proteobacteria	1	91
Pseudoalteromonas AS-43	AJ391204.1	Gamma proteobacteria	1	99
Pseudoalteromonas 2.3.053HS5R	EU267635.1	Gamma proteobacteria	1	94
Moritella WP-02–2–25	AY346334.1	Gamma proteobacteria	1	97
Vibrio viscosus	AJ132226.1	Gamma proteobacteria	1	97
U. Clostridium (B276_BX)	EF092243.1	Clostridia	3	96
U. Clostridium (TSN32)	EU302874.1	Clostridia	1	99
U. bacterium (BM89DS1BA10)	AF365631.1	Clostridia	1	90
Thalliospora MACL12B	EF198251.1	Alpha proteobacteria	2	98
U. Bacteroidetes (Pl_4t2e)	AY580708.1	Bacterioidetes	1	99
		Anaerobic decay with mud inoculums		
U. Bacteroidetes (OMEGA pl cont_7_A10)	EU052266.1	Bacterioidetes	18	92–97
U. Bacteroidetes (BBD216b_15f)	EF123557.1	Bacterioidetes	6	91–93
U. bacterium (N60e_126)	EF645953.1	Bacterioidetes	4	84–93
U. *Cytophaga*	EF657862.1	Bacterioidetes	2	87–95
U. Bacteroidetes (OMEGA pl cons (3))	EU052238.1	Bacterioidetes	1	97
U. bacterium (B01R012)	AY197383.1	Bacterioidetes	1	92
U. bacterium (BB1S16S-13)	EF433142.1	Bacterioidetes	1	98
U. bacterium (S23_534)	EF572435.1	Bacterioidetes	1	88
U. Spirochete (BBD216b_43)	EF123536.1	Spirochetales	8	91–93
U. Spirochete (WN-HWB-155)	DQ432375.1	Spirochetales	1	85
U. bacterium (ODP1227B2.10)	AB177064.1	Spirochetales	1	95
U. bacterium (LaP15L87)	EF667635.1	Caldithrix	8	83–86
U. bacterium (P. palm C 70)	AJ441232.1	Caldithrix	2	90
U. bacterium (Sm9–4)	EF582516.1	Clostridia	1	97
U. Gram-positive bacterium (K)	AB116389.1	Clostridia	1	97
U. Clostridium (B276_BX)	EF092243.1	Clostridia	1	94
Vibrio parahaemolyticus	EF467290.1	Gamma proteobacteria	1	97
Vibrio Maj4	DQ513192.1	Gamma proteobacteria	1	97
U. Gram-positive bacterium (PICO pp37)	AJ969455.1	Firmicutes	1	96
U. bacterium (Sm9–24)	EF582536.1	Firmicutes	1	99
U. delta proteobacterium (JS624–5)	AB121109.1	Delta proteobacteria	1	83
Ehrlichia TS37	AB074459.1	Alpha proteobacteria	1	87

DNA sequences were analyzed by using the BLASTN algorithm (National Center for Biotechnology Information). Identities and GenBank accession numbers indicate the highest scoring match for each clone. The percentage of sequence identity to the indicated bacteria species as determined by the BLASTN algorithm is also displayed. U., uncultured.

The relative phylogenetic simplicity of the biofilm communities we observe suggests that defined biofilms may be produced experimentally. Experimental taphonomy is well established (7), but, to date, it has focused on variables in the chemistry of the environment and the biology of the subject (6). Our results indicate that the roles of microbial processes in taphonomy must now become a major focus of research. Ideally, such experiments would use defined bacteria and conditions so that mineralized model embryos could be generated under controlled conditions. Embryos represent an ideal model system in which to investigate the principle variables underpinning decay, preservation, and mineralization in the process of fossilizing soft tissues, aiding interpretation of fossil conservation lagerstätten on which much of the narrative of animal evolutionary history is based.

Materials and Methods

Protocols for Experimental Taphonomy and Microbial Incubations. To examine the course of decay processes, embryos were killed by treatment with seawater containing 100 mmol of β-mercaptoethanol (BME) for 8–24 h and then allowed to decay under aerobic or anaerobic conditions as described below. Under these strong reducing conditions, embryos arrest after 1 to 2 cleavages or partial cleavages and autolysis does not occur (11). Taphonomy experiments were carried out at 23–25 °C.

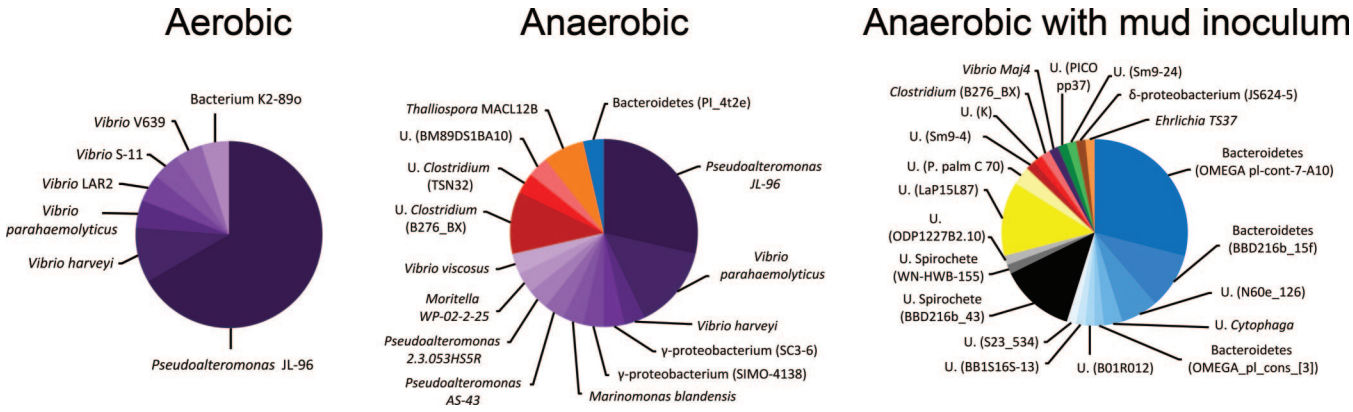

Fig. 3. Bacterial populations in prefossilization processes depend on taphonomic decay conditions. The 3 pie diagrams show bacteria identified in cloned DNA from embryos with autolysis blocked by 100 mmol of BME and then decayed for 5 days under the indicated conditions. Wedge size indicates the fraction of clones represented for each isolate. Number of clones sequenced: aerobic, 21; anaerobic, 28; anaerobic with mud inoculum, 62. Wedge color class shows bacterial group: purple, γ-Proteobacteria; blue, Bacterioidetes; green, Firmicutes; yellow, Caldithrix; orange, α-Proteobacteria; red, Clostridia; black, Spirochetales; brown, δ-Proteobacteria. U, uncultured bacteria taxa. See *Materials and Methods* for DNA preparation and analysis. See Table 1 for the complete complement of bacteria taxa present and their relative representation in each experiment.

Aerobic Decay. After 100-mmol-BME treatment, embryos were allowed to decay in seawater containing 10 mmol of BME (standard aerobic decay conditions) or just seawater with no reducing agent added. Fresh seawater piped from Sydney Harbor was kindly provided by the Sydney Aquarium. Seawater used for most experiments was prefiltered through fiberglass filter disks to remove sand and other macrosized debris, but it was otherwise untreated. However, we found that aerobic decay followed the same course as illustrated in Fig. 1 when millipore-filtered seawater was used, indicating that bacteria normally associated with marine embryos can proliferate and mediate decay. This was confirmed by the identification of bacterial species involved in decay (Fig. 3 and Table 1). Decay processes occurred faster in plain seawater than under the standard mild reducing conditions, but also followed a similar pathway.

Anaerobic Decay. Decay was examined under 2 kinds of anaerobic conditions. In standard anaerobic decay conditions, after 100-mmol-BME treatment, embryos were allowed to decay in seawater containing 10 mmol of BME in containers placed in heat-sealed plastic anaerobic bags (Bio-Bag Type A MultiPlate Environmental Chamber; catalog no. 4361216, Becton Dickinson Microbiology Systems). Oxygen indicators showed that anaerobic conditions were maintained for at least up to 9 days, the duration of the longest experiment.

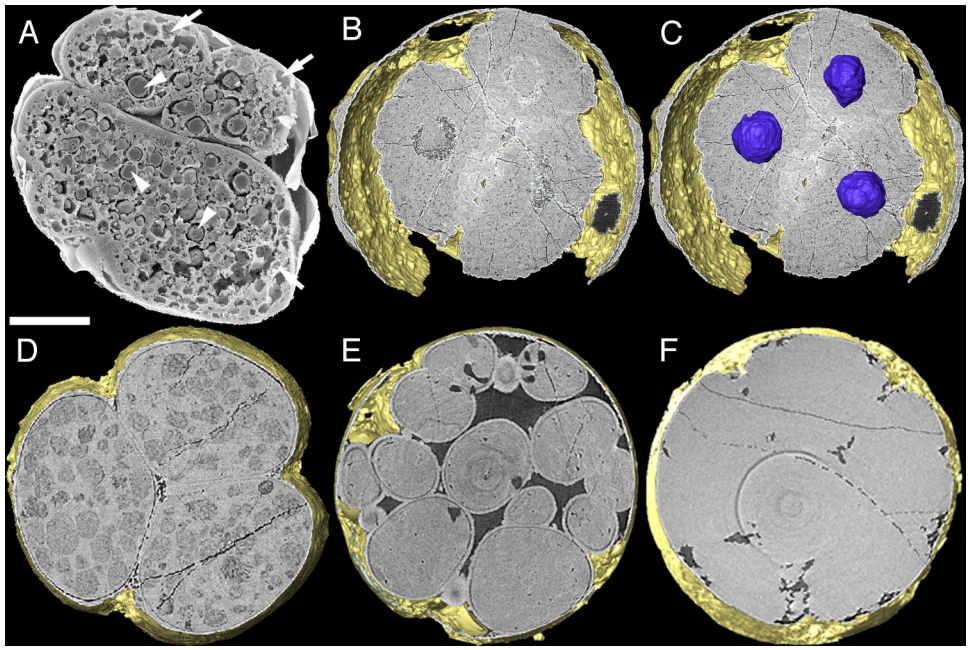

Fig. 4. Comparative internal taphonomy of recent and fossil embryos. (*A*) Cleavage stage *H. erythrogramma* embryo decayed under standard anaerobic conditions (*Materials and Methods*) for 9 days, with initial stages of biofilm development on the surface and in the outer cytoplasm. This sample was osmicated to retain the contents of lipid vesicles and shows bacterial consumption of cytoplasm: lipid is gone from vesicles near the outer cortex, where the biofilm is forming (arrows), but is still present in interior vesicles not yet reached by the biofilm (arrow heads). (*B–F*) Fossilized embryos from the Ediacaran Doushantuo Formation visualized by Synchrotron-radiation based X-ray tomographic microscopy, showing the range of preservational styles, from good to poor, respectively. Weak concentric structures are scanning artefacts. (*B* and *C*) Preserved intracellular structures representing possible cell nuclei. *B* presents an individual slice through the structures digitally rendered in *C*. (*D*) Intracellular structures comparable to the lipid droplets in the embryo from the experimental taphonomy study in *A*. (*E*) Cell walls are preserved but there are no discernible intracellular structures; interior resembles the autolyzed embryo shown in Fig. 1*C*. (*F*) Only the surface morphology of the embryo is preserved. (Scale bar: *A*, 72 μm; *B* and *C*, 148 μm; *D*, 200–250 μm; *E*, 240 μm; *F*, 287 μm).

The second type of anaerobic experiment used the same conditions plus an inoculum of anaerobic mud. Anaerobic muds were collected from different locations near Sydney; ≈24-cm mud cores were collected at low tide from sites under water at high tide; mud from the bottom 10–12 cm of the core was used for experiments. To allow retrieval, embryos in seawater containing 10 mmol of BME in vials capped with 50-μm-mesh Nitex were immersed in ≈30 mL of mud, in 50-mL beakers. Seawater containing 10 mmol of BME was added over the mud. Beakers were then placed in the anaerobic bags.

Other experiments showed that anaerobic conditions alone can prevent autolysis. Cleavage of embryos placed in anaerobic conditions arrested after a few, abnormal divisions [similar but slightly slower than treatment in 100 mmol of BME or killing with NH_4 (11)]. Anaerobic conditions for 1 day or longer blocked autolysis. Embryos returned to aerobic conditions after $<$1 day of anaerobic conditions underwent partial autolysis. After prolonged anaerobic conditions, embryos returned to aerobic conditions subsequently underwent rapid bacterial decay.

Inhibition of Bacterial Growth. Bacterial growth was inhibited by addition of rifampicin to a final concentration of 10 μg/mL (1 μL/mL of culture of a stock solution at 10 mg/mL in DMSO) in both aerobic and anaerobic conditions. A control experiment showed that DMSO at the same final concentration had no effect on embryonic cleavage or taphonomic processes.

Preparation of Bacterial DNA from Taphonomy Samples. DNA was prepared from aerobic samples and anaerobic samples with no mud inoculum by using an UltraClean Microbial DNA Isolation Kit (catalog no. 12224-50, MO BIO Laboratories). DNA was prepared from anaerobic samples with a mud inoculum by using an UltraClean Soil DNA Isolation Kit (catalog no. 12800–50, MO BIO Laboratories).

Characterization of Bacterial Species Represented in Taphonomy DNA Preparations. Lyophilized DNA from embryo samples was reconstituted in ultrapure water and then amplified by using Phusion high-fidelity DNA polymerase (New England Biolabs) and degenerative 16S rDNA oligos [forward, CACCAGAGTTTGATCMTGGTCTCAG, and reverse, TACGGHTACCTTGTTACGACTT (30)], by using 30 cycles of 10 s at 98 °C, 30 s at 60 °C, and 60 s at 72 °C. Amplicons were separated by agarose gel electrophoresis, purified by gel extraction (Qiagen), and then recombined into a Gateway Entry vector pENTR/SD/D-TOPO (Invitrogen). Positive clones were verified by restriction digestion, or PCR by using M13 and T7 specific primers, then sequenced by using an M13 oligo and BigDye Terminator v3.1 (Applied Biosystems) on an ABI Prism 3700 nucleic acid sequencer. Sequence alignments were performed by using BLASTN (National Center for Biotechnology Information).

Electron Microscopy and Electron Diffraction Methods for *Heliocidaris* Embryos. Taphonomy samples were fixed in 2.5% glutaraldehyde in Millipore-filtered seawater. *H. erythrogramma* embryos were processed for scanning electron microscopy after standard dehydration (Fig. 1) or after first postfixing in osmium tetroxide (Fig. 4), and examined on a JEOL 5800LV scanning electron microscope with a digital image archive system. *H. tuberculata* embryos for transmission electron microscopy were postfixed with osmium tetroxide, embedded in epoxy, and stained en bloc with uranyl acetate; 90-nm sections were examined with a JEOL 1010 TEM (Fig. 2). For electron diffraction, epoxy-embedded samples were examined by using selected area electron diffraction on a JEOL 1010 TEM, according to standard procedures. Images were recorded on Kodak 4489 film.

SRXTM Methodology for Fossilized Embryos. Synchrotron-radiation based X-ray tomographic microscopy (SRXTM) is a powerful nondestructive investigation method that delivers detailed volumetric information about the inner structure of samples by exploiting X-ray interactions with matter (29). For our experiment we spatially mapped the X-ray absorption of fossilized embryo specimens in 3D because the attenuation of the sample was large enough to provide sufficient contrast (Fig. 4). Our investigations were performed at the Tomography station of the Materials Science beamline (31) and at the TOMCAT beamline (32) of the Swiss Light Source at the Paul Scherrer Institute. The X-ray energy was optimized for maximum absorption contrast and the magnification of the X-ray microscope ranged from 20× to 10×. Isotropic voxels ranging between 0.35 μm and 1.75 μm have been used. Projections (501 up to 1,501, depending on magnification) were acquired equiangularly over 180°, online postprocessed, and rearranged into flat- and darkfield-corrected sinograms. Reconstruction was performed on a 20-node Linux PC farm by using highly optimized, filtered backprojection routines. Slice data derived from the scans were then analyzed and manipulated by using AMIRA (www.tgs.com) software for computed tomography.

ACKNOWLEDGMENTS. We thank Clay Fuqua (Indiana University) for help and advice on bacterial biofilms; Lisa Pratt, Juergen Schieber, and David Morgan (Indiana University) for their help with identification of bacterially produced minerals associated with decay biofilms; Jim Gehling (South Australian Museum) for his hospitality and help in understanding the fossilization of the Ediacara fauna; Else-Marie Friis (NRM Stockholm), Neil Gostling (SUNY Oswego), Amela Groso (Lausanne), Federica Marone (SLS, Villigen), and Maria Pawlowska (Cambridge) for their able assistance at the beamline; and Derek Briggs (Yale University) and Patrick Orr (University College Dublin) for helpful comments on the manuscript.

1. Bengtson S, Zhao Y (1997) Fossilized metazoan embryos from the earliest Cambrian. *Science* 277:1645–1648.
2. Xiao SH, Zhang Y, Knoll AH (1998) Three-dimensional preservation of algae and animal embryos in a Neoproterozoic phosphorite. *Nature* 391:553–558.
3. Xiao SH, Knoll AH (2000) Phosphatized animal embryos from the Neoproterozoic Doushantuo Formation at Weng'An, Guizhou, South China. *J Paleontol* 74:767–788.
4. Donoghue PCJ, *et al*. (2006) Fossilized embryos are widespread but the record is temporally and taxonomically biased. *Evol Dev* 8:232–238.
5. Steiner M, Zhu M, Li G, Qian Y, Erdtmann B-D (2004) New Early Cambrian bilaterian embryos and larvae from China. *Geology* 32:833–836.
6. Sagemann J, Bale SJ, Briggs DEG, Parkes RJ (1999) Controls on the formation of authigenic minerals in association with decaying organic matter: An experimental approach. *Geochim Cosmochim Acta* 63:1083–1095.
7. Briggs DEG (1995) Experimental taphonomy. *Palaios* 10:539–550.
8. Briggs DEG (2003) The role of decay and mineralization in the preservation of soft-bodied fossils. *Annu Rev Earth Planet Sci* 31:275–301.
9. Briggs DEG, Moore RA, Shultz JW, Schweigert G (2005) Mineralization of soft-part anatomy and invading microbes in the horseshoe crab Mesolimulus from the Upper Jurassic Lagerstatte of Nusplingen, Germany. *Proc R Soc B* 272:627–632.
10. Hagadorn JW, *et al.* (2006) Cellular and subcellular structure of neoproterozoic animal embryos. *Science* 314:291–294.
11. Raff EC, Villinski JT, Turner FR, Donoghue PCJ, Raff RA (2006) Experimental taphonomy shows the feasibility of fossil embryos. *Proc Natl Acad Sci USA* 103:5846–5851.
12. Gostling NJ, *et al.* (2008) Deciphering the fossil record of early bilaterian embryonic development in light of experimental taphonomy. *Evol Dev* 10:339–349.
13. Xiao SH, Knoll AH (1999) Fossil preservation in the Neoproterozoic Doushantuo phosphorite Lagerstatte, South China. *Lethaia* 32:219–240.
14. Hall-Stoodley L, Costerton JW, Stoodley P (2004) Bacterial biofilms: From the natural environment to infectious diseases. *Nat Rev Microbiol* 2:95–108.
15. Arp G, Reimer A, Reitner J (1999) Calcification in cyanobacterial biofilms of alkaline salt lakes. *Eur J Phycol* 34:393–403.
16. Dupraz C, Visscher PT (2005) Microbial lithification in marine stromatolites and hypersaline mats. *Trends Microbiol* 13:429–438.
17. Altermann W, Kazmierczak J, Oren A, Wright DT (2006) Cyanobacterial calcification and its rock-building potential during 3.5 billion years of Earth history. *Geobiology* 4:147–166.
18. Briggs DEG, Wilby PR (1996) The role of the calcium carbonate-calcium phosphate switch in the mineralization of softbodied fossils. *J Geol Soc* 153:665–668.
19. Pace NR, Stahl DA, Lane DJ, Olsen GJ (1986) The Analysis of natural microbial-populations by ribosomal-Rna sequences. *Adv Microbial Ecol* 9:1–55.
20. Alonso C, Pernthaler J (2005) Incorporation of glucose under anoxic conditions by bacterioplankton from coastal North Sea surface waters. *Appl Environ Microbiol* 71:1709–1716.
21. Corpe WA (1973) Microfouling: The role of primary film forming marine bacteria. *Proc. Third International Congress of Marine Corrosion and Fouling* (Northwestern Univ. Press, Evanston, IL), pp 598–609.
22. Skovhus TL, Holmstrom C, Kjelleberg S, Dahllof I (2007) Molecular investigation of the distribution, abundance and diversity of the genus Pseudoalteromonas in marine samples. *FEMS Microbiol Ecol* 61:348–361.
23. Toporski JKW, *et al.* (2002) Morphologic and spectral investigation of exceptionally well-preserved bacterial biofilms from the Oligocene Enspel formation, Germany. *Geochim Cosmochim Acta* 66:1773–1791.
24. Allison PA, Maeda H, Tuzino T, Maeda Y (2008) Exceptional preservation within pleistocene lacustrine sediments of Shiobara, Japan. *Palaios* 23:260–266.
25. McNamara ME, Orr PJ, Kearns SL, Alcalá L, Anadón P, Mollá EP, Soft tissue preservation in Miocene frogs from Libros, Spain: Insights into the genesis of decay microenvironments. *Palaios*, in press.
26. Wilby PR, Briggs DEG (1997) Taxonomic trends in the resolution of detail preserved in fossil phosphatized soft tissues. *Geobios* 30(Suppl 1):493–502.
27. Martin D, Briggs DEG, Parkes RJ (2003) Experimental mineralization of invertebrate eggs and the preservation of Neoproterozoic embryos. *Geology* 31:39–42.
28. Martin D, Briggs DEG, Parkes RJ (2005) Decay and mineralization of invertebrate eggs. *Palaios* 20:562–572.
29. Donoghue PCJ, *et al.* (2006) Synchrotron X-ray tomographic microscopy of fossil embryos. *Nature* 442:680–683.
30. Loy A, Maixner F, Wagner M, Horn M (2007) probeBase: An online resource for rRNA-targeted oligonucleotide probes: New features 2007. *Nucleic Acids Res* 35:D800–D804.
31. Stampanoni M, *et al.* (2002) High resolution X-ray detector for synchrotron-based microtomography. *Nucl Instrum Methods Phys Res A* 491:291–301.
32. Stampanoni M, *et al.* (2006) Trends in synchrotron-based tomographic imaging: The SLS experience. Developments in X-Ray tomography V, ed Bonse U. *Proc SPIE* 6318:63180M.